Optical and electrochemical properties of polyether derivatives of perylenediimides adsorbed on nanocrystalline metal oxide films

Organic Electronics 9 (2008) 757–766

Contents lists available at ScienceDirect

Organic Electronics

journal homepage: www.elsevier.com/locate/orgel

Optical and electrochemical properties of polyether derivatives of perylenediimides adsorbed on nanocrystalline metal oxide films

Mahmut Kus [a,b,*], Özgül Hakli [a,c], Ceylan Zafer [a], Canan Varlikli [a], Serafettin Demic [a], Serdar Özçelik [d], Siddik Icli [a,*]

[a] Ege University, Solar Energy Institute, 35040 Bornova, Izmir, Turkey
[b] Department of Chemistry, Mugla University, Mugla, Turkey
[c] Department of Chemistry, Celal Bayar University, Manisa, Turkey
[d] Izmir Institute of Technology, Urla-Izmir, Turkey

ARTICLE INFO

Article history:
Received 21 January 2008
Received in revised form 6 May 2008
Accepted 10 May 2008
Available online 22 May 2008

PACS:
Organic semiconductors, 72.80.L
Electrochromism, 78.20.J
Electrochromic devices, 85.60.P
Thin films optical properties 78.66

Keywords:
Perylenediimide
n-doping material
Metal oxide film
Electrochromism

ABSTRACT

We report optical and electrochemical properties of polyether derivatives of perylenediimides (PDIs) thin films formed in various materials (semiconductor, insulator, amorphous and self-assembly). Perylenediimides adsorbed on nanocrystalline TiO_2 (NT) nanocrystalline alumina (NA), amorphous silicon (PS) and neat self-assemblied (SA) films were prepared and characterized based on spectroscopic, electrochemical, spectro-electrochemical techniques. The absorption and fluorescence spectra of PDIs in chloroform exhibit vibronic features. The fluorescence quantum yields (Φ_f) of PDIs with end amino substituents in chloroform solutions are over 0.95, while the quantum yield of triethoxyphenyl substituted PDI Φ_f value is 0.024 in solution. Optical spectroscopy proves that PDIs in metal oxide thin films form aggregated type complexes. An electrochromism, a color change from red to blue/violet, is observed on metal oxide films, that indicates existence of mono and dianion forms of PDIs. Reversibility of electrochemical reductions in NT film depends on the scanning rate. However, electrochromism in NA films is stable and reversibility is independent from scanning rate. Stable mono and diaionic species are formed on NA films. SA films show broad absorption peaks during the voltammetric scan. On the other hand, the first reduction onset potentials of PDIs are almost equal to the onset potential of capacitive current of TiO_2 which lead to low efficiency in dye-sensitized solar cells.

1. Introduction

Perylenediimides (PDIs) represent one of the most widely studied classes of organic semiconductors with possible applications in photovoltaic cells, electrophotography, laser dyes and organic light-emitting diodes [1–8]. They are inexpensive and easily accessible materials also attractive owing to intense, high fluorescence quantum yield and general photostability but suffer from poor solubility in common organic solvents. Synthesis of highly soluble PDIs is very important for the preparation of their thin films to be used in photoelectronic applications [9–11]. They exhibit singlet energy transfer over unusually long distances [12,13]. Most organic conducting materials can be described as p-type semiconductors; in contrast, PDIs are described as n-type semiconductors in which the major charge carriers are in their conduction band. Such materials are employed as electron accepting materials in all organic photovoltaic solar cells [7,8,14–18]. PDIs show two reversible electrochemical reductions at modest potentials,

* Corresponding authors. Address: Selcuk University, Department of Chemical Engineering, 42100 Konya, Turkey. Tel.: +90 332 2232095; fax: +90 332 2410635 (M. Kus), Tel.: +90 232 3886025; fax: +90 232 3886027 (S. Icli).
E-mail addresses: mahmut_kus@yahoo.com (M. Kus), siddik.icli@ege.edu.tr (S. Icli).

1566-1199/$ - see front matter © 2008 Elsevier B.V. All rights reserved.
doi:10.1016/j.orgel.2008.05.009

leading to the formation of stable anions and dianions [19]. This property of PDIs makes them attractive materials in chemiluminescence, near-infrared emitters and electrochromic devices [14,16,20]. The majority of studies on optical and electrochemical properties of PDIs are carried out in solution [16,19,21] and the number of solid state electrochemistry studies are limited [15,22–25]. Additionally, macroscopic oxide films are under intensive investigation due to their use in optoelectronic applications such as dye-sensitized solar cells, electrochromic and electroluminescent displays [26–33]. The electrochemistry of self-assembly films of polyether derivatives of PDIs was previously reported by Gregg [25], but we could find no report on the electrochemistry of polyether substituted PDI doped nanocrystalline metal oxide films.

On the other hand, the research field of electrochromic materials includes organic, inorganic, and polymeric materials as well as several hybrid materials [34,35]. The most common applications of EC materials include a variety of displays, smart windows, optical shutters, and mirror devices. Electrochromic materials include organic small molecules, such as the bipyridiliums (viologens), which are a class of materials that are transparent in the stable dicationic state. Electrochromism is observed for the thin films of polyviologens and N-substituted viologens such as heptyl viologen [34]. Recently, improved electrochromic properties have been observed with composite systems, where organic molecules are adsorbed on mesoporous nanoparticles of doped metal oxides [35,36–38]. To the best of our knowledge, electrochromic effect of perylenediimides adsorbed on mesoporous surfaces was not reported. Previously, we reported spectroelectrochemical properties of perylenemonoimidemonoanhydride derivatives but not for perylenediimides [38,39].

In this paper, series of PDI derivatives are synthesized, electrochemical and spectral behavior of PDIs on nanocrystalline metal oxide particles are investigated. The stability of mono and dianionic species on mesoporous metal oxide surface is presented. PDI 1–4 include polyether side chain ending with amino groups and PDI 5 includes phenyl substituted polyether side chain attached from phenyl units to perylene core. Free amino substituents are chosen for their reactive features that allow functionalization and/or they provide a site for attaching on different substrates. Phenyl substituted polyether derivative is chosen for its low fluorescent feature and compare with PDI 1–5. In order to determine the solid state behavior of synthesized dyes, the optical and electrochemical properties are studied on semiconductor (nc-TiO_2), insulator (nc-Al_2O_3), amorphous Si surfaces and self-assembly films and that compared with their solutions in $CHCl_3$ The chemical structures and their names of synthesized PDIs are given in Scheme 1.

2. Experimental section

2.1. Chemicals and instruments

Perylene-3,4:9,10-tetracarboxylic dianhydride (PDA), tetraethylene glycol di(*p*-toluene sulphonate) (TEGdTs), pentaethylene glycol di(*p*-toluene sulphonate) (PEGdTs), sodium (Na), ethanolamine, 1-amino-2-propanol, triethylene glycol monomethyl ether, aluminum oxide (neutral) and silicagel 60 for column chromatography, tetrabutylammonium hexafluorophosphate ([TBA][PF_6]), titanium (IV) isopropoxide [Ti(O^iPr)$_4$], poly(ethyleneoxide) (MW 100.000), glacial acetic acid, tetraethyl orthosilicate (TEOS) were obtained from Fluka. Potassium carbonate (K_2CO_3), dimethyl formamide (DMF), *p*-nitrophenol (*p*-NO_2PhOH), hydrazine monohydrate ($NH_2NH_2.H_2O$), imidazole, thionyl chloride ($SOCl_2$), benzene, and pyridine were obtained from Merck. Organic solvents chloroform ($CHCl_3$), dichloromethane (CH_2Cl_2), acetonitrile (MeCN), ethanol (EtOH), methanol (MeOH), 2-propanol (^{i}PrOH), tetrahydrofuran (THF), ethyl acetate (EtOAc), toluene ($C_6H_5CH_3$) were of spectroscopic grade and used as received. Ferrocene (Fc) was from Aldrich and used as standard for the determination of LUMO energy levels of synthesized PDI derivatives.

PDI derivatives were analyzed by using Nicolet Magna 550 FTIR spectrophotometer, Bruker DPX-400 and 400 MHz HP Digital FT–NMR spectrometer, Analytic Jena S 600 UV spectrophotometer, PTIQM1 fluorescence spectrophotometer and Picoquant Time-Harp 100 instrument equipped with PDL 800-B laser/LED pulse lamb. CH Instruments 660B model potentiostate was used for electrochemical measurements under nitrogene atmosphere at various scan rates. Tencor Alpha Step 500 profilometer was used in thickness measurements of the films.

2.2. Synthetic methods

PDIs were synthesized according to the published literature procedures [41a–d].

2.3. Preparation of PDI doped nanocrystalline titania film (NT)

The nanocrystalline TiO_2 films were prepared according to the procedure described in literature [42a]. The autoclaving process was carried out at 235 °C, instead of 200 °C and colloidal solution condensed to 10% by weight of TiO_2. Anatase TiO_2 colloids were obtained from a sol-gel hydrolysis by autoclaving and condensation of Ti(O^iPr)$_4$ in acetic acid solution. 160 ml of H_2O and 51 ml glacial acetic acid were mixed in a flask and stirred at 0 °C. 6 ml of ^{i}PrOH and 24 ml Ti(O^iPr)$_4$ were mixed in a dropping funnel. The Ti(O^iPr)$_4$ / ^{i}PrOH solution was dripped into acetic acid-H_2O mixture, which was previously prepared and kept at 0 °C, at a rate of 1–2 drops/s. The mixture was refluxed for 4 h and then recovered colloidal solution was placed into an autoclave chamber equipped with a Teflon beaker and heated at 235 °C for 12 h. After this treatment the colloidal solution was sonicated and evaporated to a final concentration of 10% of TiO_2 by weight. In order to act as a binding agent poly(ethyleneoxide), 20% by weight with respect to the amount of TiO_2, was added to this final colloidal solution. The paste was coated onto microscope glass slides by doctor blade technique. TiO_2 films were dried at room temperature and then sintered at 450 °C for 30 min. Final thickness of porous TiO_2 films were ~5 μm. Doping of the PDIs onto TiO_2 films were performed by soaking

glass slides into 0.5 mM MeCN solution of PDIs and keeping in the solution for 3 h. PDI adsorbed TiO_2 films finally washed with fresh MeCN.

2.4. Preparation of PDI doped silica films (PS)

TEOS (22.4 ml, 0.1 mol) and dry EtOH (11.2 ml) were mixed in a flask and stirred for 10 min under N_2 atmosphere (Solution A). A mixture of 7.2 ml H_2O (0.4 mol) and 1 ml HCl (37%) were added to absolute EtOH (11.2 ml) in a flask and stirred for 10 min (Solution B). Solution A was added dropwise to Solution B that was under vigorous stirring. Synthesized PDIs were dissolved in this sol–gel solution to obtain 0.5 mM final dye concentration. After obtaining an individual complete dissolution of each PDI, 1 ml Triton-X 100 surfactant was added to sol–gel solution in order to prevent the films from cracking. After stirring for 5 min, resulting silica sol-gel solution was coated onto microscope glass slides by dip coating. The films were dried at 100 °C for 30 min. Final thickness of silica films were measured and found to be ~4.5 μm.

2.5. Preparation of PDI doped nanocrystalline alumina film (NA)

Nanocrystalline Al_2O_3 (alumina) films were prepared by Yoldas et. al. route [42b]. Aluminium tri-*iso* propylate (51 g 0.25 mole) hydrolyzed in 450 ml (25.5 mole) hot water at 75–80 °C under vigorous stirring. 1.46 ml (0.0175 mole) HCl (36.5%) added into solution and peptized for 3 days at 90 °C. At the end a clear solution (sol) was obtained. The sol was concentrated to 17.5% Al_2O_3 (w/w) at 50 mbar and 50 °C with rotary evaporator. 8% PEG 20000 was added to obtain a better film and stirred overnight to get homogeneous paste. The paste was coated on the conductive FTO coated glass electrodes by doctor blade technique. Scotch 3M Polymer tape was used as a spacer. Prepared films were heated at 500 °C for 30 min. Thickness of the films was found as 8 μm.

2.6. Preparation of self-assembly PDI films (SA)

THF solutions of the PDIs with a concentration of 15–20 mg PDI/ml THF were used for spin-coating (1600 rpm). Glass microscope slides were used as support material.

3. Results and discussion

Synthesized PDIs were waxy and very soluble in common organic solvents ranging from alcohols to toluene. Their solubility in polar and protic solvents was better than aprotic and non-polar ones. This might be because of the polar side chains of the dyes and their capability of making hydrogen bonds with protic solvents.

3.1. Absorbance and luminescence properties of PDIs

The absorption and fluorescence spectra of the PDIs were recorded in four different organic solvents ($C_6H_5CH_3$, $CHCl_3$, MeOH, and MeCN) and four different thin

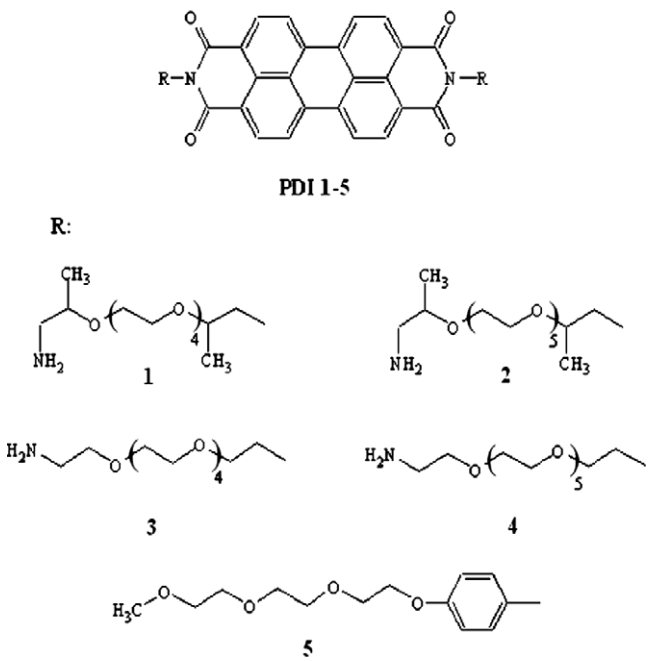

Scheme 1. N,N′-Bis{2-[2-(2-{2-[2-(2-amino-1-methylethoxy) ethoxy]ethoxy}ethoxy) ethoxy] propyl}-perylene-3,4:9,10- tetracarboxydiimide, (PDI 1); N,N′-bis(2-{2-[2-(2-{2-[2-(2-amino-1-methylethoxy)ethoxy]ethoxy}ethoxy)ethoxy]ethoxy}propyl)-3,4:9,10-perylene tetracarboxydiimide, (PDI 2); N,N′-bis{2-[2-(2-{2-[2-(2-aminoethoxy)ethoxy]ethoxy}ethoxy)ethoxy]ethyl}-3,4:9,10-perylene tetracarboxydiimide, (PDI 3); N,N′-bis(2-{2-[2-(2-{2-[2-(2-aminoethoxy)ethoxy]ethoxy}ethoxy)ethoxy] ethoxy}ethyl)-3,4:9,10-perylene tetracarboxydiimide, (PDI 4); N,N′-bis(4-{2-[2-(2-methoxyethoxy) ethoxy]ethoxy}phenyl)-3,4:9,10-perylene tetracarboxydiimide, (PDI 5).

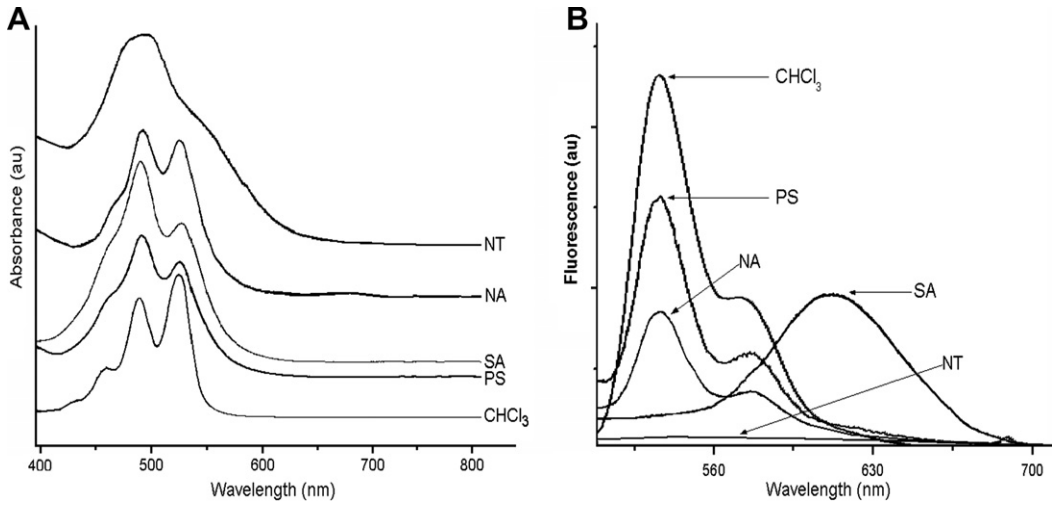

Fig. 1. (A) Absorption spectra of PDI 3 in $CHCl_3$, PS, SA, NA and NT films and (B) fluorescence emission spectra of PDI 3 in $CHCl_3$, and the films (PS: silica film, SA: self-organized film, NT: nanocrystalline titania film, and NA: nanocrystalline alumina film).

films (NT, PS, self-assemblied (SA), and NA) at room temperature. Fig. 1A shows the absorption spectra of PDI 3 in $CHCl_3$ solution and films. The UV–vis absorption spectra of the PDIs in solution have three bands at 459, 488 and 522 nm, which are characteristic for all symmetric PDI derivatives [1–5]. The maximum absorption and fluorescence emission wavelengths of the PDIs have slightly blue-shifted (about 5–6 nm) with increasing solvent polarity. Strong broadening of absorption peaks due to exciton–phonon coupling was observed in the case of film and the absorption maximum shifts blue by 0.21 eV (from 522 to 488 nm) due to the π-orbital overlaps between dye molecules [44]. The broadening of the absorption spectrum was mostly dominant in NT films when compared to NA, PS and SA films. The absorption maxima are changed from 522 to 488 nm whenever the dye environment is changed from $CHCl_3$ solvent to film matrix. Although the nature of this shift is not very well known, it is related to the intermolecular interactions and aggregation tendency of these dyes in thin films [45–48]. The ratio of absorbances of 522 to 488 nm band decreases, which often indicates aggregation of these dye molecules [48].

The fluorescence emission spectra (Fig. 1B) of PDIs were obtained in $CHCl_3$ solutions ($\lambda_{exc} = 488$ nm) and in thin films. The emission spectra of the PDI derivatives were all the same except the SA and NT films. In SA and NT films, the three emission bands that are characteristic for PDIs were seen. The emission spectra of SA films were broadened and strongly red-shifted, whereas the emission in NT films was almost disappeared (Fig. 1B).

The fluorescence quantum yields (Φ_f) of PDIs in $CHCl_3$ were calculated according to the published procedure and N-DODEPER was used as the reference [43]. The Φ_f of the PDIs in $CHCl_3$ was determined as 0.95–1.0 for PDI 1–4, however for PDI5 this value was calculated as 0.024. Determinations of fluorescence quantum yields of the dyes in solution are relatively easy in comparison to thin films. In thin films many corrections, such as self-quenching of the emission and the total internal reflection of the emission due to high refractive indices must be done for acceptable determination of quantum efficiencies. On the other hand, Tirapattur et al. calculated the fluorescence quantum yield by using time-resolved fluorescence measurements obtained in both phases (solution and thin films) assuming that the fluorescence decay constants (k_f) are similar in both phases [49,50]. But this approach may not be valid since the fluorescence decays are multi exponentials.

Fig. 2 shows fluorescence decay curves (bir tane decay var) of PDI 3 in $CHCl_3$ solution. The fluorescence lifetimes (τ_f) were measured to be 5, 17, 2.8 and 1.7 ns in solution ($CHCl_3$), and in the SA, PS and NA films, respectively (Table 1). The fitting procedure applied to the fluorescence decay profiles yield acceptable statistic ($X^2 < 1.2$) with a single-exponential function in $CHCl_3$ solutions and multi exponentials in thin films.

The red-shift observed for PDIs in SA films was about 90 nm. Liu et al. observed that PDIs including polyether side chains form highly ordered thin films [51]. The strong tendency of PDIs to form π–π stacking arrangement may yield strong interactions between PDIs in the films resulting in a red-shift in spectra and a longer fluorescence lifetime [52]. Similar red-shifted emission band was observed for PDI polymers by De Witte et al. [53]. The fluorescence lifetime of SA films are measured to be between 15.7–18.2 ns, which are significantly longer than those in $CHCl_3$. The longer fluorescence lifetime in SA films is in agreement with literature and explained by the formation of excimer type species in films [48,53] The experimental data clearly points that the presence of new species which could be an excimer type of aggregates or complexes of PDIs in SA films. The fluorescence spectra of PDIs in PS and NA thin films are similar to those in solutions but lower in fluorescence intensity. Furthermore, the fluorescence lifetimes of PDIs in PS and NA thin films are shorter than those of in solution and measured to be 2.8 and 1.7 ns for PS and NA films, respectively. Shorter lifetimes are consisted with

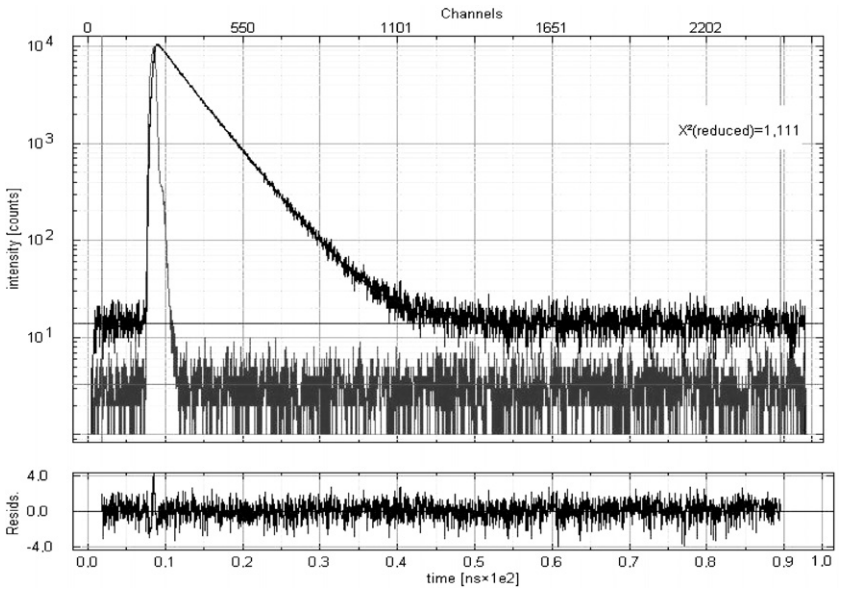

Fig. 2. The fluorescence decay curve of PDI 3 (in $CHCl_3$, concentration $<10^{-5}$).

Table 1
Spectroscopic data for the PDIs in solution and thin films

PDI	τ_f (ns)				Φ_f
	$CHCl_3$	SA	PS	NA	$CHCl_3$
1	4.74	18.2	2.85	1.78	0.99
2	4.99	16.3	2.78	1.76	0.95
3	4.72	15.7	2.81	1.82	1.00
4	4.67	17.3	2.92	1.77	0.99
5	0.06	–	–	–	0.024

τ_f values are fluorescence lifetimes and Φ_f values are quantum yields.

lower intensity of fluorescence, pointing that rate of nonradiative transitions, regardless of their nature, are faster than the radiative transitions. The low Φ_f of PDI 5 arises from the electron-rich aromatic substituent, which leads to a strong fluorescence quenching, as reported and described in literature [32,33,54–58]. It must be noted that, the fluorescence lifetime of PDI 5 in PS and NA films were not reported because of poor statistics even with multiexponential decay curves.

Extremely weak fluorescence intensity of the synthesized PDIs may be attributed to the strong electrostatic interactions between TiO_2 and dye molecules [59]. It also indicates the possibility of efficient photo-energy/electron transfer processes from the excited PDI molecules to the nanostructured TiO_2 surface. Bossman et al. reported that $Ru(bpy)_3^{2+}$ complexes located near TiO_2 do not emit light [60]. HOMO and LUMO energy levels of $Ru(bpy)_3^{2+}$ (−5.9 and −3.9 eV) [40] are very similar to those of PDIs, (−5.9 and −3.8 eV) [54]. The quenching mechanism of our dyes can be explained by the injection of excited electrons to electron traps below the band edge of TiO_2. Thus the injected electrons recombine by non-radiative processes resulting in a very weak emission and very fast fluorescence decay that is faster than our instrument response. Solid state electrochemical studies support our approach and these results will be discussed in following sections.

3.2. Electrochemistry of PDIs in solution

Determination of HOMO and LUMO energy levels is crucial for the selection of anodic and cathodic materials in organic electronics [61]. Electrochemical potentials provide these information. The electrochemical measurements of PDIs were performed by the use of 0.1 M $[TBA][PF_6]$ as electrolyte in $MeCN/CHCl_3$: 5/1 solvent mixture. Glassy carbon electrode (GCE) was used as working, platinum wire as counter and Ag/AgCl as reference electrodes. Calculation of LUMO and HOMO energy levels were based on the value of 4.8 eV for ferrocene with respect to vacuum level and following equations were used [62]

$$E_{LUMO} = -e(E_{1/2(red.,dye)} - E_{1/2(Fc)} + 4.8),$$
$$E_{HOMO} = -e(E_{1/2(ox.,dye)} - E_{1/2(Fc)} + 4.8).$$

The onset potentials ($E_{red.1}$ and $E_{red.2}$) were determined from the intersection of two tangents drawn at the rising reduction current and background current in the cyclic voltammograms. The first reduction peak was used to calculate the LUMO energy level as it belongs to the reduction of neutral molecule whereas the second peak belongs to the reduction of monoanion of parent molecule. HOMO energy values of PDIs were estimated from oxidation potentials. The electrochemical band gap values are calculated by subtracting the onset potential of the first reduction and the first oxidation.

Two reversible reductions of PDIs are observed on the voltammograms. The redox potentials and HOMO–LUMO energy levels of the dyes are given in Table 2. The cyclic voltammogram of PDI 1 in $CHCl_3$ solution (as inset) is shown in Fig. 3. Two reversible reduction peaks around −0.57 and −0.77 V and one irreversible oxidation peak

Table 2
Peak potentials of PDIs in $CHCl_3$ and films

PDI	$E_{ox.}$ (V)	$E_{red.1}$ (V)				$E_{red.2}$ (V)				LUMO (eV)[c]	HOMO (eV)[c]	Band gap (eV)
	$CHCl_3$	$CHCl_3$	SA	NT	NA	$CHCl_3$	SA	NT	NA	$CHCl_3$	$CHCl_3$	$CHCl_3$
1	+1.68	−0.57	−0.81	−0.85	−0.84	−0.77	−1.07	−1.15	−1.06	−3.95	−6.07	2.25[a] 2.12[b]
2	+1.72	−0.56	−0.82	−0.83	−0.86	−0.75	−1.05	−1.16	−1.09	−3.96	−6.14	2.24[a] 2.18[b]
3	+1.73	−0.54	−0.80	−0.85	−0.85	−0.72	−1.05	−1.13	−1.05	−3.93	−6.12	2.25[a] 2.19[b]
4	+1.79	−0.53	−0.79	−0.85	−0.82	−0.74	−1.07	−1.15	−1.10	−3.95	−6.07	2.25[a] 2.12[b]
5	+1.60	−0.58	−0.76	−0.88	−0.86	0.72	−1.09	−1.19	−1.08	−3.88	−6.06	2.25[a] 2.18[b]

[a] Optical band gaps.
[b] Electrochemical band gaps.
[c] (Fc/Fc^+ is 0 and 42 V vs Ag/AgCl).

around 1.68 V are observed for PDI 1. The peak separations between two reduction potentials are 14–20 mV. ΔE_p values are 79 mV for first reduction and 82 mV for second reduction. Integration of peak shapes shows that each reduction refers to one electron process. No significant change at the peak currents is observed after several cycles (15 times). LUMO energy values of PDIs in solution are calculated to be between −3.88 and −3.96 eV. The electrochemical and optical band gap values are in good correlation and observed to be between 2.1 and 2.3 eV (Table 2). Although the LUMO energy levels, calculated from the redox potentials for liquid phase seem to be favorable for photovoltaic applications, the solid state electrochemistry data is required to support it. That is why the position of conduction band edge of TiO_2 is dependent on the amount the ions adsorbed at inner Helmholtz double layer of TiO_2/electrolyte interface [63]. The amount of ions, adsorbed at Helmholtz layer, maybe, is affected by the adsorbed dye on TiO_2 surface. The electrochemistry of the thin films will be discussed in Section 3.3.

3.3. Electrochemistry of thin films

Solid state electrochemistry is a useful tool to understand whether there is an interaction between electroactive groups of organic molecule and metal oxide surfaces or not. NA, SA and NT films were prepared on FTO glasses and used as working electrode. Fig. 3 shows cyclic voltammetry of SA, NT an NA films. Since PDI 1–4 are soluble in common solvents, the SA films of them are not stable in electrolyte and just only one cyclic scan can be performed with high scan rates (⩾200 mV/s). However, the very low solubility of PDI 5 in CH_3CN allowed us to make the spectroelectrochemical experiments in SA films. Therefore, the results in SA films were given and discussed only for PDI 5.

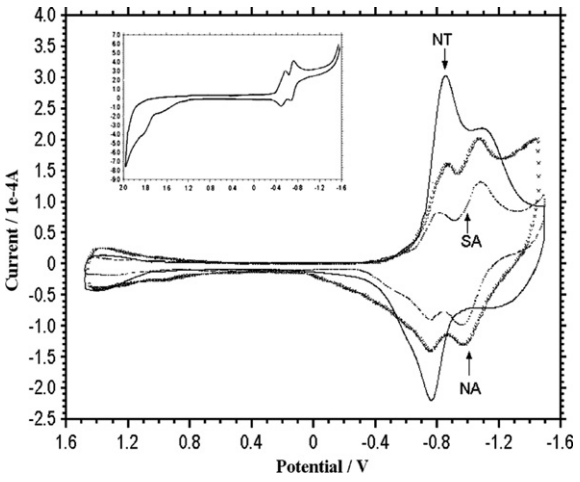

Fig. 3. Cyclic voltammogram of NT (PDI 1), NA (PDI 1) and SA (PDI 5) films. The inset is cyclic voltammogram of PDI 1 in solution (supporting electrolyte is 0.1 M [TBA][PF_6] in MeCN/$CHCl_3$:5/1).

The redox potentials of films shows approximately 25 mV negative shift when compared with solution phase. This shift may be explained by the limited percolation of electrolyte cations. TBA^+ cations are quite large and its percolation inside the film is more difficult than that of smaller cations, such as Li^+, Na^+ etc. Gregg et al. reported that, because of its large size and the nonreactive alkyl groups on its periphery, TBA^+ neither adsorbs on the TiO_2 surface nor reacts chemically with it [64]. On the other hand, polyether side chain oxygen atoms with unpaired electrons may be attractive centers for electrolyte cations. Electrostatic interactions between electrolyte cations and unpaired electrons on oxygen atoms may decrease the mobility of cations. In order to understand this approach better, amino precursor (PEGDA1), which contains pentaethyoxy chain and non-electroactive in studied potential region, is doped onto TiO_2 film and electrochemical behavior of the films are monitored. Fig. 4 shows the cyclic voltammograms of bare TiO_2, bare alumina and PEGDA1 doped TiO_2 films. The alumina films show a weak background current but it is negligible in comparison with that of TiO_2 film. The TiO_2 films show a capacitive current starting from −0.60 V. Because of the electron traps below bulk conduction band edge of TiO_2, the electrons flow from F:SnO_2 electrode to TiO_2 particles. These accumulated electrons are immobile unless they are thermally excited to the conduction band [65]. The capacitive current of TiO_2 film slightly increases when doped with PEGDA1. As mentioned above, polyether side chains including oxygen atoms may act as attractive centers for electrolyte cations. Although TBA^+ cations do not like TiO_2 surface, the etheric oxygens may facilitate their movement though the film surfaces that results in more capacitance.

CV measurements were also carried out by using $LiClO_4$ as electrolyte and the results (not shown here) supported our approach. Influence of electrolyte cations on redox behavior is another topic for future studies. Here, we fo-

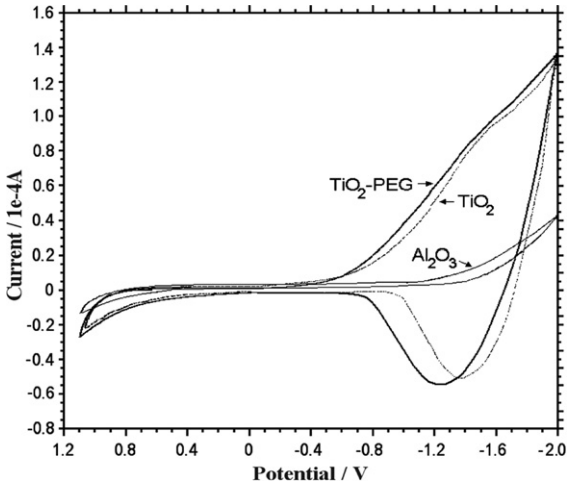

Fig. 4. Cyclic voltammogram of bare TiO_2, alumina and amino precursor (PEGDA1) doped TiO_2 film.

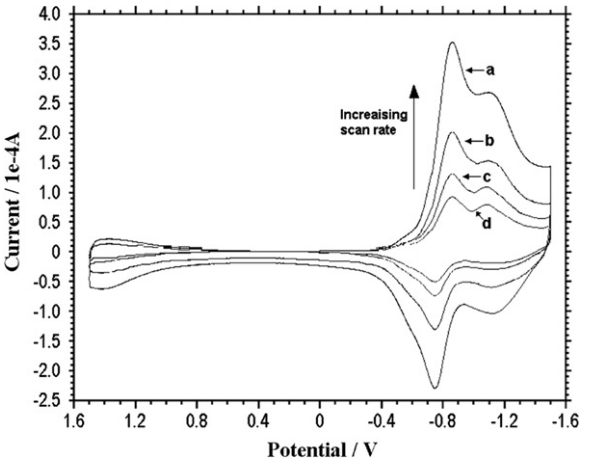

Fig. 5. Cyclic scans of PDI 5 at 200 (a), 100 (b), 50 (c) and 25 (d) mV/s scan rate.

cused on the influence of the film matrix on redox behaviors. Therefore, the potentials in 0.1 M $TBAPF_6$ were considered.

As expected, SA and NA films show two reversible reductions. The reduction peaks are separated by ~30 mV. The peak separations are ~15 mV larger than that of solution phase. This can be attributed to a dimer anion ($dimer^-$) formation between monoanion and neat perylene molecules after the first reduction step. Thus, the formation of dianion becomes more difficult (requires more negative voltage) in SA and NA films. The NT films show different behavior during voltammetric time scale. The second reduction onset voltage shifts slightly to more negative potentials than those of SA and NA films. Moreover, the first reduction is reversible but the reversibility of the second reduction changes depending on the scan rate. Integration of the peaks shows that approximately 30% of monoanion does not convert to dianion. The onset potential of capacitive current on NT films is nearly at the same potential with that of PDIs and the electron accumulation on TiO_2 particles continues during the voltammetric scan. The first reduction onset of PDI may not be influenced by the accumulated electrons due to the small amount of accumulation. However the amount of accumulated electrons increases by the increasing negative voltage and this may supply some negative charge for positively charged non-reduced carbonyl groups. Thus the second reduction potentials of PDI might be expected to shift more negative potentials than those of SA and NA films. Reversibility of the reduction waves depends on the scan rate in NT films. The reduction waves are almost fully reversible at high scan rates (>100 mV/s). However, the oxidation waves disappear when the scan rate is decreased (Fig. 5). At very low scan rates, desorption of adsorbed PDI is also observed. The cyclic scans at various (5, 10, and 25 mV/s) scanning rates shows that the desorption starts below −1.0 V that approximately corresponds to the second reduction peak of PDI. We applied −1.0 V for 3 min to a 2 cm^2 TiO_2 film in order to desorb enough amount of dye to the solution phase that will allow cyclic scan. The cyclic voltammogram of the desorbed dye gave only one reversible reduction peak at around −0.5 V. It indicates that a degradation process exists after the second reduction. Gosztola et al. observed some degradation of PDI dianion during bulk electrolysis in OTTLE cell and they attributed that some residual oxygen in OTTLE cell can lead a photodegradation process [20]. Since SA and NA films did not show such degradation in our working condition, it is clear that TiO_2 plays an active role. We think that the PDIs, presented in this study, are not convenient for Greatzel type organic dye-sensitized photovoltaic applications since the onsets of capacitive current of TiO_2 and the first reduction of PDI are nearly at the same potential. That is why the onset of capacitive current is related with the Fermi level of TiO_2 and it is clear that the LUMO energy level of PDIs lies under the conduction band of TiO_2. It is a known the fact that the LUMO level of dye must be located slightly above the conduction band edge of n-type semiconductor for electron injection [26].

3.4. Spectroelectrochemistry of thin films

The changes in absorption spectra of the films depending on applied voltage were also characterized. Spectroelectrochemical measurements were carried out with NT and NA films. The working electrode was $F:SnO_2$ – metal oxide – PDI with ~1 cm^2 area. The counter and quassi-reference electrodes were prepared by stripping 5 mm of $F:SnO_2$ coating in the middle of the $F:SnO_2$ coated glass, and coating the separated parts by platinum and silver paste, respectively. The working electrode and counter/quassi-reference electrode were sealed with surlyn agent at 110 °C. Nitrogen saturated supporting electrolyte was filled from previously prepared holes to system under vacuum. The prepared systems were placed into the holder of UV–vis spectrophotometer and connected to potentiostat.

Both NA and NT films display striking electrochromism during the reduction process. A color change from red to blue and from blue to violet is observed while the potential decreases from 0 to −1.8 V. Blue color appears at the first

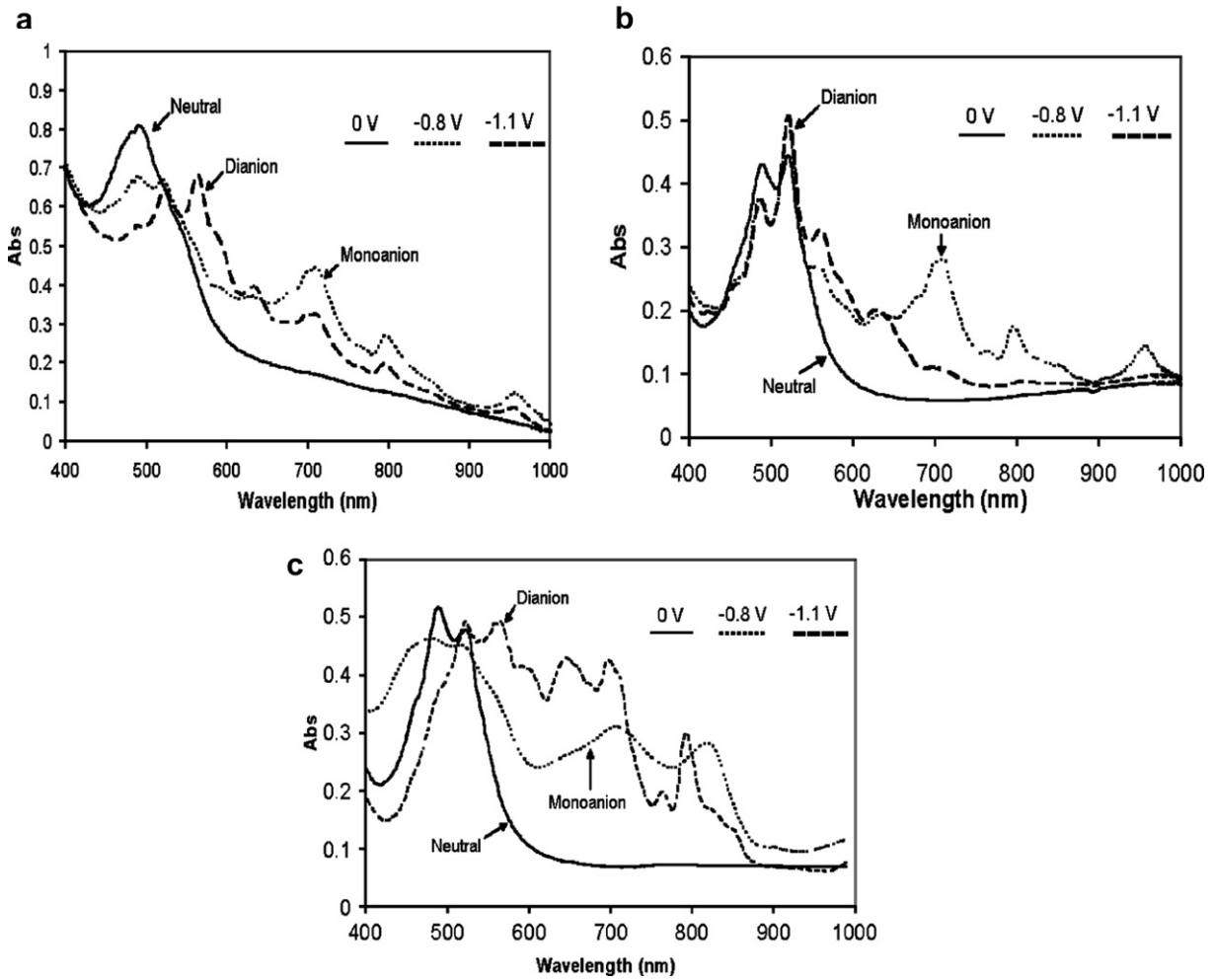

Fig. 6. Absorption spectra of NT–PDI 1 (a), NA–PDI 1 (b) and SA–PDI 5 (c) films with respect to applied voltage.

reduction potential which correspond to monoanion. The color change from blue to violet (dianion) appears down to −1 V. Several cycles were carried out at high scan rates (>100 mV/s) and complete color change is observed in both NA and NT films. However, due to possible degradation of the dye at NT films, color loss occurs at scan rates lower than 100 mV/s. At more positive potentials (∼0 V) compared to the offset of monoanion re-oxidation potential, color change from violet to red is observed in NT films. No additional peak corresponding to color change observed. That means, the electrons do not move to F:SnO_2 electrode, probably remain in TiO_2 traps, thus no current (or peak on cyclic scale) appears. The form of cathodic and anodic current in bare TiO_2 electrode supports our approach (Fig. 4). While the cathodic scan shows a linear increase, the anodic scan shows peak-like discharge of accumulated electrons. The offset of anodic scan is observed to be more negative than the onset of the cathodic scan. It indicates that the discharge of accumulated electrons occurs faster than accumulation. Thus, most of the traps become empty before the complete oxidation of monoanions of PDI. On the other hand, the color change is reversible in NA films. The complete color change from blue (monoanion) to red (neutral) terminates close to 0 V. In agreement with color change, the oxidation peak tail appears up to 0 V in NA films (Fig. 3). These observations also indicate that TiO_2 particles mostly capture a couple of electrons given by monoanion under the negative voltage. Fig. 6 shows the absorption spectra of NA and NT films with respect to the applied voltage conditions. New absorption peaks at 631, 674, 710, 773, 796 and 956 nm grow up to −1.0 V. These are characteristic monoanion peaks as reported by other authors, with the exception that the peak at 631 nm does not decline by the applied voltage below −1.0 V [20,25,66]. As mentioned above, ∼30% of monoanion remains in NT films. Therefore the absorption peaks related to monoanion is observed below −1.0 V which is onset potential for dianion formation. By the formation of dianions, the peaks at 523, 563 and 590 nm are observed. The maximum absorption band of dianion in NA films appears at 523 nm, while this value is 563 nm in NT films. The peak at 523 nm is characteristic maximum absorption band for dianion of PDI in solution [20]. As discussed above, the degradation of PDI starts by the forma-

tion of dianion. The decrease of the characteristic absorption maxima is due to the degradation of PDIs. The NA films show similar absorption bands of dianion formation in solution. The peaks corresponding to neutral species still appear during the monoanion formation in NA and NT films. It is most probably due to the formation of dimeric species between monoanion and neutral species.

The absorption spectra of SA films (for PDI 5) show structureless and broad peaks especially for dianion. The absorption spectra of monoanion show more or less definable broad peaks. By the formation of monoanion, the absorption peaks of neutral PDI become broad and new broad peaks appear at 700 and 820 nm. The peaks become more complicated by the formation of dianion. Self-assembly films of PDIs which are chemically reduced show similar results [45].

4. Conclusion

In this study, electrochemical and spectroscopic properties of polyether derivatives of PDIs adsorbed on metal oxide surface are presented. Electrochromism of PDIs is clear and stable on NA films. The observation of red and blue color in the systems presented in this study, especially in NA films, maybe an advantage for the design of RGB molecular electrochromic devices. On the other hand, the onset potential of the first reduction LUMO of PDIs and the onset potential of capacitive current (Fermi level) of TiO_2 are almost equal. It indicates the LUMO level of PDIs is under the conduction band of TiO_2. Therefore, these dyes may not be convenient for photovoltaic applications.

Acknowledgements

We acknowledge partial funding by the European Commission (FP6 MOLYCELL project-SES-CT-2003-502783), Scientific and Technical Research Council of Turkey (TUBITAK, NATO A-2 support funds) and Alexander von Humbolt Foundation of Germany. We appreciate the project support funds of the State Planning Organization of Turkey (DPT).

References

[1] H. Langhals, S. Sprenger, M.T. Bradherm, Liebigs Ann. (1995) 481.
[2] H. Langhals, W. Jona, Eur. J. Org. Chem. (1998) 847.
[3] K.D. Belfield, K.J. Schafer Jr., M.D. Alexander, Chem. Mater. 12 (2000) 1184.
[4] A.M. Van de Craats, J.M. Warman, P. Schlichting, U. Rohr, Y. Greets, K. Müllen, Synth. Met. 102 (1999) 1550.
[5] P. Pösch, M. Thelakkat, H.W. Schmidt, Synth. Met. 102 (1999) 1110.
[6] W. Huang, D. Yan, Q. Lu, Y. Huang, Eur. Polym. J. 39 (2003) 1099.
[7] Y. Shibano, T. Umeyama, Y. Matano, H. Imahori, Org. Lett. 9 (2007) 1971.
[8] T. Edvinsson, C. Li, N. Pschirer, J. Schöneboom, F. Eickemeyer, E. Sens, G. Boschloo, A. Herrmann, K. Müllen, A. Hagfeldt, J. Phys. Chem. C Lett. 111 (2007) 15137.
[9] H. Icil, S. Icli, J. Polym. Sci. A: Polym. Chem. 35 (1997) 2137.
[10] M.J. Ahrens, L.E. Sinks, B. Rybtchinski, V. Liu, B.A. Jones, J.M. Giaimo, A.V. Gusev, A.J. Goshe, D.M. Tiede, M.R. Wasielewski, J. Am. Chem. Soc. 126 (2004) 8284.
[11] S. Mackinnon, M.Z.Y. Wang, J. Polym. Sci. A: Polym. Chem. 38 (2000) 3467.
[12] H. Dincalp, S. Icli, J. Photochem. Photobiol. A: Chem. 141 (2001) 147.
[13] C. Karapire, C. Timur, S. Icli, Dyes Pigments 50 (2003) 135.
[14] M.E. Williams, R.W. Murray, Chem. Mater. 10 (1998) 3603.
[15] G. Tamizhmani, J.P. Dodelet, Chem. Mater 3 (1991) 1046.
[16] W. Lu, J.P. Gao, Z.Y. Wang, Y. Qi, G.G. Sacripante, J.D. Duff, P.R. Sundararajan, Macromolecules 32 (1999) 8880.
[17] C.W. Struijk, A.B. Sieval, J.E.J. Dakhorst, M. Van Dijk, P. Kimkes, R.B.M. Koehorst, H. Donker, T.J. Schaafsma, S.J. Picken, A.M. Van de Craats, J.M. Warman, H. Zuilhof, E.J.R. Sudhölter, J. Am. Chem. Soc. 122 (2000) 11057.
[18] R.A. Cormier, B.A. Gregg, J. Phys. Chem. B 101 (1997) 11004.
[19] S.K. Lee, Y. Zu, A. Herrmann, Y. Geerts, K. Müllen, A.J. Bard, J. Am. Chem. Soc 121 (1999) 3513.
[20] D. Gosztola, M.P. Niemcyzk, W. Svec, A.S. Lukas, M.R. Wasielewski, J. Phys. Chem. A 104 (2000) 6545.
[21] W.E. Ford, H. Hiratsuka, P.V. Kamat, J. Phys. Chem 93 (1989) 6692.
[22] K.J. Cho, H.K. Shim, Y.I. Kim, Synth. Met. 117 (2001) 153.
[23] J. Danziger, J.P. Dodelet, N.R. Armstrong, Chem. Mater. 3 (1991) 812.
[24] D.K. Slattery, C.A. Linkous, N.E. Gruhn, J.C. Baum, Dyes Pigments 49 (2001).
[25] B.A. Gregg, R.A. Cormier, J. Phys. Chem. B 102 (1998) 9952.
[26] B. O'Reagan, M. Gratzel, Nature 353 (1991) 737.
[27] M. Graetzel, Nature 414 (2001) 338.
[28] Q. Wang, S. Zakeeruddin, .M. Cremer, J. Baeuerle, P. Humphry-Baker, R.M. Graetzel, J. Am.Chem. Soc 127 (2005) 5706.
[29] P. Bonhote, E. Gogniat, F. Campus, L. Walder, M. Graetzel, Displays 20 (1999) 137.
[30] Y.S. Huang, L. Kavan, I. Exnar, M. Graetzel, J. Electrochem. Soc. 142 (1995) L142.
[31] W. Gopel, K.D. Schierbaum, Sens. Actuators B 26 (1995) 1.
[32] M.T. Möller, S. Asaftei, D. Corr, M. Ryan, L. Walder, Adv. Mater. 216 (2004) 1558.
[33] R. Cinnsealach, G. Boschloo, S.N. Rao, D. Fitzmaurice, Sol. Energ. Mater. Sol. Cells 55 (1998) 215.
[34] C.A. Bignozzi, M. Biancardo, P.F.H. Schwab, Semiconductor photochemistry and photophysics, in: V. Ramamurthy, K.S. Schanze (Eds.), Molecular and Supramolecular Photochemistry, vol. 10, Marcel-Dekker, New York, 2003.
[35] A.A. Argun, P.H. Aubert, B.C. Thomson, I. Schwendeman, C.L. Gaupp, J. Hwang, N.J. Pinto, D.B. Taner, A.G. MacDiarmit, J.R. Reynolds, Chem. Mater. 16 (2004) 4401.
[36] M. Biancardo, P.F.H. Schwap, R. Argazzi, C.A. Biagnozzi, Inorg. Chem 42 (2003) 3966.
[37] D. Corr, U. Bach, D. Fay, M. Kinsella, C. McAtamney, F. O'Reilly, S.N. Rao, N. Stobie, Solid State Ionics 165 (2003) 315.
[38] U. Bach, D. Corr, D. Lupo, F. Pichot, M. Ryan, Adv. Mater. 14 (2002) 845.
[39] M. Kus, S. Demic, C. Zafer, G. Saygili, H. Bilgili, S. Icli, Eur. J. Phys.: Appl. Phys. 37 (2007) 277.
[40] K. Ocakoglu, C. Zafer, B. Cetinkaya, S. Icli, Dyes and Pigments 75 (2007) 385.
[41] (a) D.J. Chadwick, I.A. Cliffe, I.O. Sutherland, J. Chem. Perkin Trans. I 565 (1984) 1707;
(b) C.J. Pedersen, J. Am. Chem. Soc. 89 (1967) 7017;
(c) J.P. Dutasta, J.P. Declerg, C.E. Calderon, B. Tirant, J. Am. Chem. Soc. 111 (1989) 7136;
(d) B.H. Langhals, W. Jona, F. Einsield, S. Wahnlich, Adv. Mater. 10 (1998) 1022.
[42] (a) M.G. Kang, N.G. Park, Y.J. Park, K.S. Ryu, S.H. Chang, Solar Energ. Mater. Solar Cells 75 (2003) 475;
(b) B.E. Yoldas, J. Am. Ceram. Soc. Bull. 54 (1975) 286.
[43] C. Karapire, C. Zafer, S. Icli, Synth. Met. 2145 (2004) 51.
[44] Y. Luo, J. Lin, J. Coll. Int. Sci. 297 (2006) 625.
[45] R.O. Marcon, S. Bronchsztain, Langmuir 23 (2007) 11972.
[46] B. Janey, S.K. Asha, J. Phys. Chem. B 110 (2006) 20937.
[47] E.M. Calzado, J.M. Villalvilla, P.G. Boj, J.A. Quintana, R. Gomez, J.L. Segura, M.A. Diaz-Garcia, J. Phys. Chem. C. 111 (2007) 13595.
[48] R. Gomez, D. Veldman, R. Blanco, C. Seoane, J.L. Segura, R.A.J. Janssen, Macromolecules 40 (2007) 2760.
[49] S. Tirapattur, M. Belletete, N. Drolet, M. Leclerc, G. Durocher, Chem. Phys. Lett. 370 (2003) 799.
[50] S. Tirapattur, M. Belletete, N. Drolet, M. Leclerc, G. Durocher, Macromolecules 35 (2002) 8889.
[51] (a) S.G. Liu, G. Siu, R.A. Cormier, R.M. Leblane, B.A. Gregg, J. Phys. Chem. B 106 (2002) 1307;
(b) R.A. Cormier, B.A. Gregg, Chem. Mater. 10 (1998) 1309.
[52] C. Burgdorff, H.G. Löhmannsröben, R. Reisfeld, Chem. Phys. Lett. 197 (1992) 358.
[53] P.A.J. De Witte, J. Hernando, E.E. Neuteboom, E.M.H.P. van Dijk, S.C.J. Meskers, R.A.J. Janssen, N.F. van Hulst, R.J.M. Nolte, M.F. Garcia-Parajo, A.E. Rowan, J. Phys. Chem. B. 110 (2006) 7803.
[54] D. Uzun, M.E. Ozser, K. Yuney, H. İcil, M. Demuth, J. Photochem. Photobiol. A: Chem. 156 (2003) 45.

[55] Y. Liu, S. Xiao, H. Li, Y. Li, H. Liu, F. Lu, J. Zhuang, D. Zhu, J. Phys. Chem. B 108 (2004) 6256.
[56] H. Quante, Y. Geerts, K. Müllen, Chem. Mater. 9 (1997) 495.
[57] M.O. Vysotsky, V. Bohmer, F. Wurthner, C.C. You, K. Rissanen, Org. Lett. 4 (2002) 2901.
[58] K.D. Belfield, M.V. Bondar, O.V. Przhonska, K.J. Schafer, J. Photochem. Photobiol. A: Chem. 151 (2002) 7.
[59] G. Ramakrishna, H.N. Ghosh, J. Phys. Chem. B 105 (2001) 7000.
[60] S.H. Bossman, C. Turro, C. Schnabel, M.R. Pokhrel Jr., L.M. Payavan, B. Baumeister, M. Wörner, J. Phys. Chem. B 105 (2001) 5374.
[61] A.R. Watkins, J. Phys. Chem. 78 (1974) 2555.
[62] D.O. Cowan, R.L.E. Drisko, J. Am. Chem. Soc. 192 (1970) 6281.
[63] B.A. Gregg, S.G. Chen, R.A. Cormier, Chem. Mater. 16 (2004) 4586.
[64] B.A. Gregg, Si-G. Chen, S. Ferrere, J. Phys. Chem. B 107 (2003) 3019.
[65] H.G. Agrell, G. Boschloo, A. Hagfelt, J. Phys. Chem. B 108 (2004) 12388.
[66] R.O. Marcon, S. Brochsztain, Langmuir 23 (2007) 11972.